This is the accepted manuscript of the following article: A. Bedoya, M. Colom, A. Mendioroz, A. Salazar, E. Marín, *Measurement of the thermal conductivity of fluids using laser spot lock-in thermography*, **Measurement** 158 : (2020) // Article ID 107740, which has been published in final form at https://doi.org/10.1016/j.measurement.2020.107740. © 2020 Elsevier under CC BY-NC-ND license (http://creativecommons.org/licenses/by-nc-nd/4.0/)

MEASUREMENT OF THE THERMAL CONDUCTIVITY OF FLUIDS USING LASER SPOT LOCK-IN THERMOGRAPHY

A. Bedoya[1,2], M. Colom[2], A. Mendioroz[2], A. Salazar[2], E. Marín[1,+]

[1] *Instituto Politécnico Nacional, Centro de Investigación en Ciencia Aplicada y Tecnología Avanzada (CICATA) Unidad Legaria, Legaria 694, Colonia Irrigación, Delegación Miguel Hidalgo, Ciudad de México 11500, México.*

[2] *Departamento de Física Aplicada I, Escuela de Ingeniería de Bilbao, Universidad del País Vasco, UPV/EHU, Pza. Ingeniero Torres Quevedo 1, 48013 Bilbao, Spain*

[+] *Corresponding author: emarinm@ipn*.mx

Abstract

In this work, we propose a new method to retrieve the thermal conductivity of fluids, k_f, using laser spot lock-in infrared thermography. The measurement cell consists in two paralepidid blocks separated by a narrow gap of variable and known width, L. This gap can be filled with a gas or a liquid, producing a thermal contact resistance, R_{th}, which quantifies the thermal barrier to heat propagation. By focusing the laser spot close to the interface between the two solids, this thermal contact resistance can be obtained by fitting the temperature field recorded by the infrared camera to its analytical expression. Using the well-known relationship $R_{th} = L/k_f$, the thermal conductivity of the fluid is obtained from a simple linear relation. Measurements performed in test samples show a good agreement between determined thermal conductivities and literature reported values, demonstrating the validity of the method.

Key words: Laser spot lock-in infrared thermography; thermal conductivity; fluids; thermal resistance; interfacial layer

1. Introduction

The knowledge of the thermal conductivity of fluids is important not only from a point of view of basic research, but also in several technological applications where heat transfer is prevalent, such as heat exchangers, thermal insulation and refrigerant processes. Several methods have been proposed for thermal conductivity measurement in fluids, such as the parallel-plate, the steady-state cylindrical cell, the temperature oscillation, the 3ω, the thermal comparator and the transient hot wire. A critical review of these techniques is given by Paul *et al* [1], who showed that the latter is the most accepted and extensively used at present. This is because of the high accuracy it provides and its capacity to eliminate the errors due to convective effects that are always present in these samples, due to the existence of buoyancy forces. The transient hot wire [2] is a direct method in which a very thin metal wire is immersed in the sample and acts as both a heating unit and a temperature sensor. The thermal conductivity is evaluated directly from the slope of the linear region of the curve relating the temperature rise of the wire to the logarithm of time. Among the limitations of the method are the difficulty to select the linear interval of the mentioned curve that matches the conditions imposed by the theoretical model describing the technique [3], the relative high volume of sample required, the complexity of the electronic apparatuses involved and the delicacy of the thin wire that limited the commercial development of hot wire instruments [4].

Laser spot lock-in infrared thermography has proven to be an efficient non-contact method to measure thermal transport properties of solids [5], but to the best of our knowledge has not been used for thermal characterization of gases and liquids. However, a recently proposed application of this technique [6] for measurement of the thermal contact resistance at the vertical interface between two solid materials inspired us to propose a new method for thermal conductivity measurements in fluids that fill the interfacial cavity. In this paper, we describe the theoretical and experimental details behind this method, whose usefulness is demonstrated by measurements of the thermal conductivity of air, water and ethylene-glycol, some of the most common fluids.

2. Experimental and theoretical basis of the method

Figure 1 shows the experimental procedure presented in Ref. [6]. Two parallelepiped blocks of different materials with mirror like polished surfaces are brought very close to each other leaving a micrometric air gap of width L between them. The surface of one of the two blocks (piece 2) is heated by a focused laser beam of power P_o

and radius a, whose intensity is periodically modulated at an angular frequency $\omega = 2\pi f$, where f is the modulation frequency. The distance between the laser and the interface is d. The amplitude of the surface temperature field is recorded using a thermographic camera with lock-in incorporated facilities. The analytical expression of the surface temperature along a line perpendicular to the interface and crossing the center of the laser spot (the y-axis of Fig. 1) is given in [6], where heat losses by convection and radiation were neglected

$$T_1(0,y,0) = \frac{P_o}{\pi}\int_0^\infty e^{-\frac{(\delta a)^2}{16}} I_o\left[\frac{(\delta a)^2}{16}\right] e^{\left(\frac{\alpha^2\beta_2^2}{8} - \beta_2 d + \beta_1 y\right)} f_1(\delta)\delta d\delta \qquad y<0 \qquad (1a)$$

and

$$T_2(0,y,0) = \frac{P_o}{2\pi k_2}\int_0^\infty \delta J_o(\delta|y-d|)\frac{e^{-\frac{(\delta a)^2}{8}}}{\beta_2} d\delta + \\ + \frac{P_o}{2\pi}\int_0^\infty e^{-\frac{(\delta a)^2}{16}} I_o\left[\frac{(\delta a)^2}{16}\right] e^{\left(\frac{\alpha^2\beta_2^2}{8} - \beta_2 d - \beta_2 y\right)} f_2(\delta)\delta d\delta \qquad y>0 \qquad (1b)$$

where

$$f_1(\delta) = \frac{1}{k_1\beta_1 + k_2\beta_2 + R_{th}k_1\beta_1 k_2\beta_2}, \qquad (2a)$$

$$f_2(\delta) = \frac{1}{k_2\beta_2} \times \frac{-k_1\beta_1 + k_2\beta_2 + R_{th}k_1\beta_1 k_2\beta_2}{k_1\beta_1 + k_2\beta_2 + R_{th}k_1\beta_1 k_2\beta_2}, \qquad (2b)$$

$\beta_j = \sqrt{\delta^2 + q_j^2}$, $q_j = \sqrt{i\omega/D_j}$ is the thermal wave vector, j = 1,2. D_j and k_j are the thermal diffusivity and conductivity of the j-th medium respectively, J_o is the Bessel function of order zero, I_o is the modified Bessel function of order zero and δ (m^{-1}) is the conjugated variable of the radial coordinate, r, in the Hankel space.

Fitting the experimental temperature amplitude profile along the y-axis to the above analytical expression allows to retrieve the value of R_{th} (m^2KW^{-1}), the thermal contact resistance of the interface, defined as the ratio between this temperature drop and the average heat flux per unit area across the interface. In Ref. [6] the vertical interface was filled with air, and this procedure was used to measure the width of the interface, using the expression

$$R_{th} = \frac{L}{k_f}, \qquad (3)$$

where k_f is the (known) thermal conductivity of the fluid filling the interface. Rth represents

In this work, we propose to measure the thermal resistances corresponding to different known interface widths to obtain, from a simple linear fitting to Eq. (3), the thermal conductivity of the fluid that fills the interface.

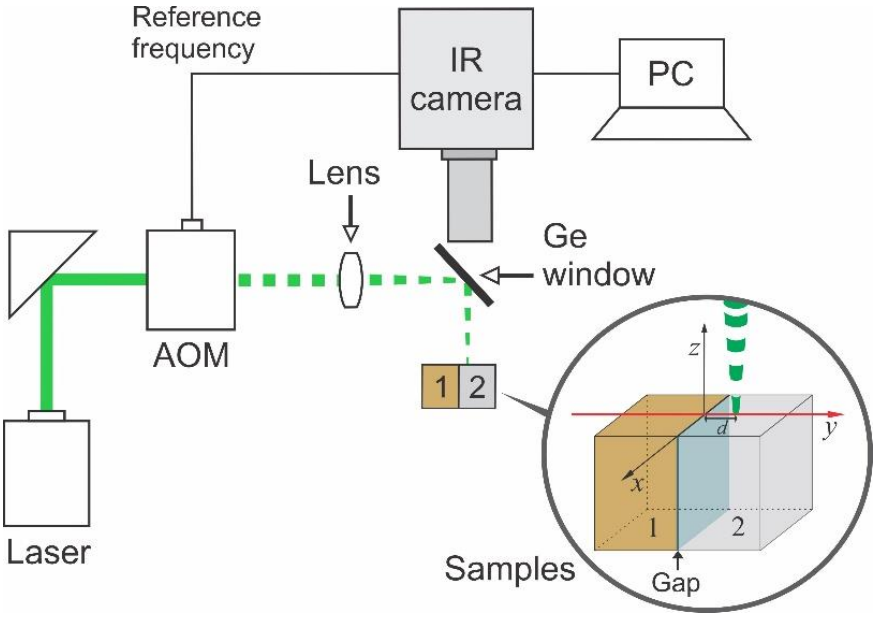

Fig. 1. Schema of the experimental set-up, where AOM stands for Acousto-Optic Modulator. The inset shows the geometry of the sample.

In order to illustrate the methodology, we took the data reported in Ref. [5] corresponding to interfaces of different widths between Poly-Ether-Ether-Ketone (PEEK) and AISI-304 stainless steel, filled with air. In Fig. 2 we plot the nominal values of the interface widths (L) as a function of the retrieved thermal resistances (R_{th}). The straight line is the best linear fit to Eq. (3), whose slope gives the air thermal conductivity. In this way, we obtained a value of k_f = 0.0257 ± 0.0008 $Wm^{-1}K^{-1}$, in agreement with the literature one, k_{air} = 0.026 $Wm^{-1}K^{-1}$ [7]. The measurement uncertainty (≈ 3%) is adequate for thermal conductivity measurements [8]. This result proves that the thermal conductivity of air can be measured using this methodology, and suggests a new method for measuring the thermal conductivity of fluids, by filling with them the interfacial cavity of what we will call from now “the measurement cell” (denoted as sample in Fig. 1).

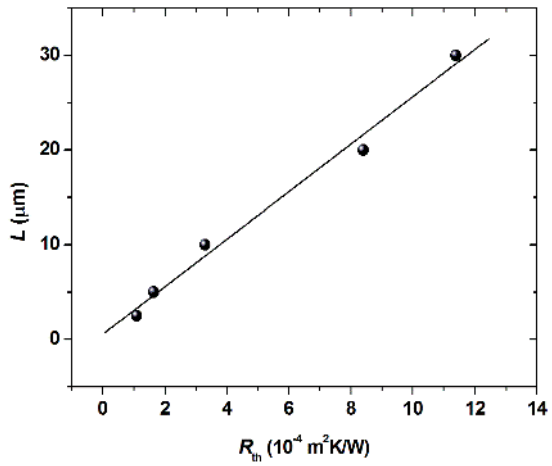

Fig. 2. Nominal value of the air gap width as a function of the retrieved thermal resistance for a PEEK-AISI-304 system. Dots are the experimental data and the solid line is the linear fit.

3. Numerical calculations and sensitivity analysis

Although Eqs. 1 provide the general expressions of the temperature profiles along the *y*-axis when the materials at both sides of the fluid are different; the methodology is simpler if the same material is used to build the measurement cell. Accordingly, in the following we set $D_1 = D_2 = D$, and $k_1 = k_2 = k$ in Eqs. 1, and we analyze three solids of low, intermediate and high conductivity: PEEK, AISI-304 and Aluminum, respectively.

Figure 3 shows computer calculations of the natural logarithm of the temperature amplitude profiles, using Eqs. (1), for a measurement cell composed of two pieces of AISI-304 stainless steel. Two fluids (air and water) filling the interfacial layer are considered. Calculations were performed for four different widths of this layer corresponding to realistic values of the measurement cell. Values of the whole set of parameters used in the calculations are shown in Table 1. Note that for each sample the laser power is selected in order to produce a similar maximum temperature rise of about 30 K. As can be observed in Fig. 3, an abrupt jump, ΔT, is observed in the temperature at the interface, which increases with the gap width. However, for the same interface width the temperature jump at the discontinuity is higher for air than for water. This result is related to the fact that ΔT depends on R_{th}, which, according to Eq. (3), is the ratio L/k_f. Accordingly, for the same interface width, the higher the fluid conductivity the smaller the temperature jump at the interface. On the contrary, the difference in the temperature

jumps for the extreme gap widths considered (5 and 40 μm) is larger for water than for air. Therefore, there is plenty of room to select a large range of gap thicknesses in the experiments in order to plot nominal thickness versus retrieved thermal resistance to estimate the thermal conductivity of the fluid accurately.

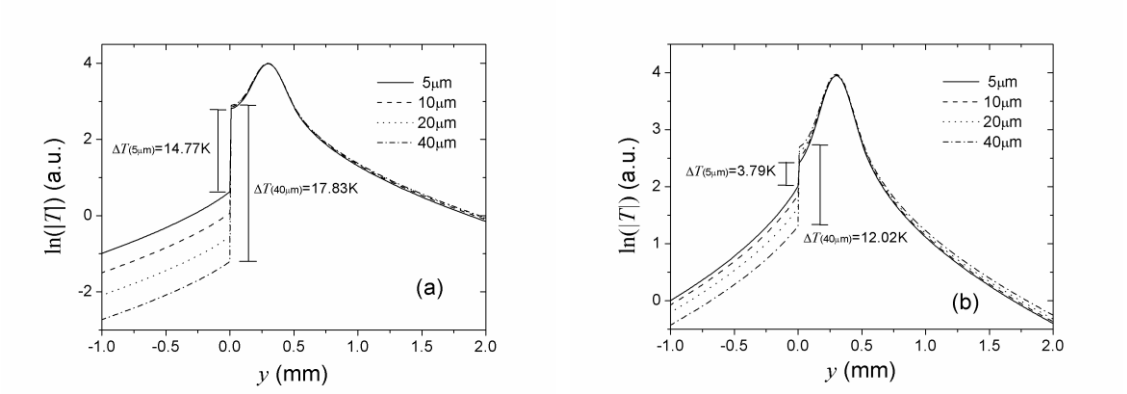

Fig. 3. Computer calculation of the natural logarithm of the temperature amplitude profiles along the *y*-axis for a system composed of two pieces of AISI-304 stainless steel with (a) air (k_{air}= 0.026 $Wm^{-1}K^{-1}$), and (b) water (k_{water}= 0.6 $Wm^{-1}K^{-1}$ [9]) as the substance filling the gap layer, for different gap widths.

Table 1. Values of the parameters used in the computer simulations.

Parameter	**Material**		
	AISI-304	**PEEK**	**Al**
k ($Wm^{-1}K^{-1}$)	14.92 [10]	0.259 [11]	238 [7]
D (m^2s^{-1})	4×10^{-6} [12]	0.18×10^{-6} [11]	93×10^{-6} [7]
P_o (W)	0.3	6.8×10^{-3}	4.7
a (m)	150×10^{-6}		
d (m)	300×10^{-6}		
f (Hz)	0.5		
L (m)	$(5, 10, 20, 40) \times 10^{-6}$		

In order to select the best solid material to build the experimental cell, we perform a sensitivity analysis of the dependence of ΔT on k_f. In Fig. 4 we show the computer calculations of ΔT as a function of k_f for the three solids we are dealing with: AISI-304, PEEK and Al, and the same gap widths as in Fig. 3, between 5 and 40 μm. We can see

that the curves for different widths are monotonous, but they move in the direction of increasing k_f when the width of the gap rises. As can be seen, the region of highest sensitivity (largest change of ΔT when varying k_f) is different for each solid. In particular, the k_f value with the highest sensitivity increases with the thermal conductivity of the solid: for PEEK, a poor thermal conductor, the highest sensitivity is around $k_f = 10^{-2}$ $Wm^{-1}K^{-1}$; for AISI-304, an intermediate thermal conductor, the highest sensitivity is around $k_f = 10^{-1}$ $Wm^{-1}K^{-1}$ and for Al, a good thermal conductor, the highest sensitivity is around $k_f = 2$ $Wm^{-1}K^{-1}$. Note, however, that in the case of aluminum, the power required to obtain amplitude values at the surface like those of PEEK and AISI 304 is very high, and thus this option lacks practical interest. As all fluids and gases are in the thermal conductivity range from 10^{-2} to 1 $Wm^{-1}K^{-1}$, AISI-304 stainless steel is the best choice for building the experimental cell.

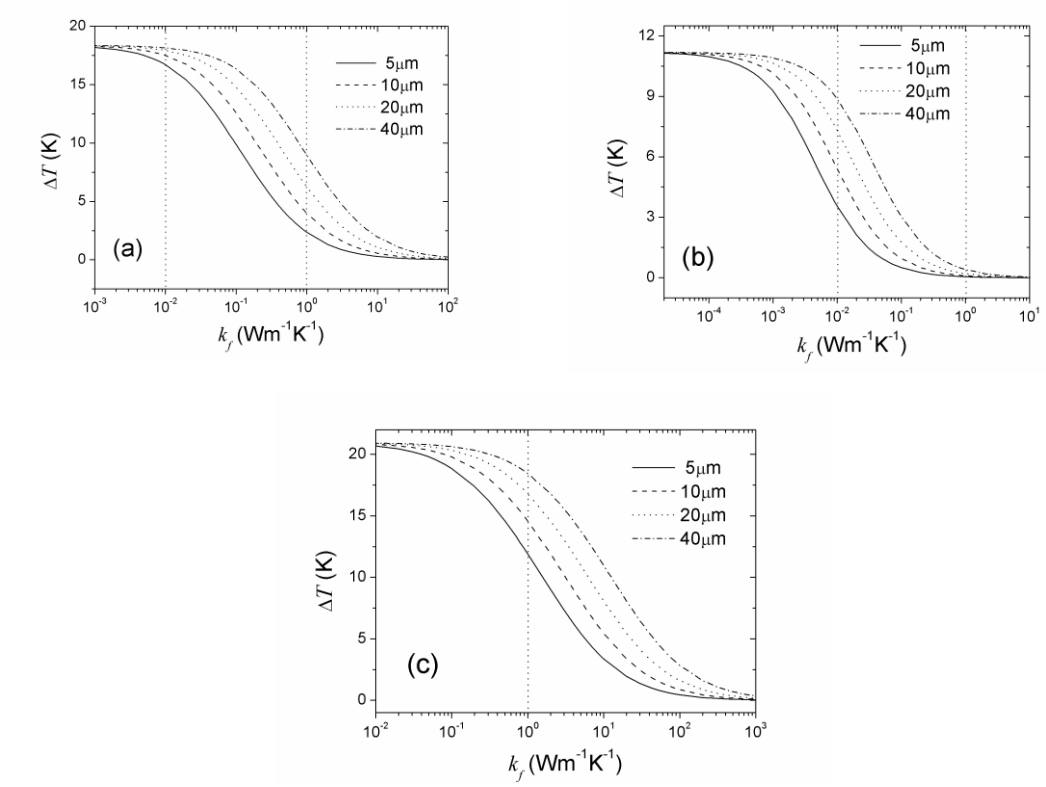

Fig. 4. Computer calculations of ΔT versus k_f for measurement cells made of (a) AISI-304, (b) PEEK and (c) Al. Dotted lines represent the k_f range of all liquids and gases.

4. Experimental results and discussion

According to the sensitivity study of the previous section, the measurement cell is made of AISI-304 stainless steel cubes of 3 cm side. As the methodology has already

been assessed in section 2 with air, an extremely poor thermal conductor, we have chosen as test fluids a high thermal conductivity and universal liquid, water, (k_{water} = 0.6 $Wm^{-1}K^{-1}$) [8] and ethylene glycol ($k_{ethil\text{-}glyc}$ = 0. 258 $Wm^{-1}K^{-1}$) [13] as an intermediate conductivity liquid.

The experimental set-up is the same depicted in Fig. 1, where the CW laser is a Verdi-V6 from COHERENT (532 nm and up to 6 W) and the infrared camera is a SC7000 from FLIR, with a 320 x 256 pixel detector working in the 3.5 – 5 μm range, and noise equivalent temperature difference (NETD) of 20 mK. The absolute temperature measurement was not calibrated as only relative values are relevant to determine the thermal resistance. A microscope lens (x1) allows improving the spatial resolution up to 30 μm. Images were captured at a frame rate of 200 frames per second, with an integration time of 825 μs. By averaging 15000 images in the lock-in process, we reduce the average noise in amplitude down to 0.3 mK [14].

The measurement cell, instead, was improved in order to achieve different widths of the interfacial layer using a single cell. Figure 5 shows the diagram of the new configuration, showing the wedged gap between two pieces of stainless steel, which was obtained by sandwiching two metallic sheets of different thicknesses (denoted in Fig. 5 as L_A and L_B), between the steel blocks, close to the ends. A moderate pressure was applied to the blocks to maintain the different parts together but taking care to avoid false contact. The laser and the camera positions were fixed, while the sample was displaced using a micrometer stage along *x*-axis with a 2 mm step. Due to the wedged shape of the cavity, for each position of the sample the interface width at the location of the laser spot is different. Even if the theoretical model describes a homogenous interface, the effect of the wedge angle is negligible as it is smaller than 0.1º in all data sets. Furthermore, temperature data used for quantification of the thermal resistance is restricted to the profile that crosses the center of the laser spot. We have verified that this temperature *y*-profile in the wedged sample is indistinguishable from the profile obtained in a sample with parallel surfaces separated by a width equal to the separation of the wedged sample at the position of the laser spot. The retrieved thermal resistances coincide within the experimental uncertainty.

The sample surface was always kept perpendicular to the optical axis of the camera. The temperature amplitudes along the transverse *y*-profile crossing the interface through the center of the laser spot were recorded for different widths L_i of the gap. These

gap widths were determined by measuring the thicknesses L_A and L_B, the distance between the metallic sheets and the displacement of the sample. Taking into account the uncertainty in these distances, the resulting uncertainty in the estimation of the interface widths L_i is 2 μm. Typical values of laser power, radius and distance to the interface were P_o = 200 mW, a = 170 μm and d = 390 μm, respectively. These values were selected according to the sensitivity analysis presented in Ref [6]. A very thin graphite layer, about 5 μm thick, was sprayed at the surface of the sample (x-y plane) to enhance and homogenize the infrared emissivity over the entire surface, besides of increasing the absorption of the excitation beam.

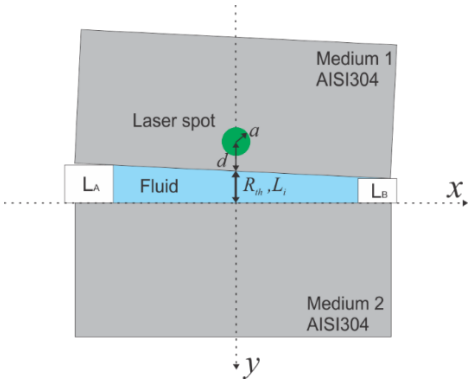

Fig. 5. Diagram of the measurement cell showing the separating sheets used to construct the wedged gap between the two AISI-304 stainless steel blocks.

In Fig. 6 we show the results for water. Measurements have been performed at f = 0.3 Hz. Figure 6a shows a typical amplitude thermogram when the laser excites the surface at a position where the water thickness is L = 60 μm. In figure 6b we plot the natural logarithm of the temperature amplitude profiles along the y-axis for four widths (L = 70, 56, 41 and 26 μm). Dots are the experimental data and the continuous lines are the multiparametric fittings to Eqs. 1 using a Levenberg-Maquard algorithm in Matlab with four free parameters: P_o, d, a, and R_{th}. The retrieved R_{th} values are inserted in the figure, together with the confidence intervals of the nonlinear regression. The values of parameters d, a, and P_o are of less interest. However, they allowed verifying the quality and consistency of the fitting as they were in excellent agreement with the preset experimental conditions. Note that the graphs are shifted along the vertical axis to better appreciate the jumps at the interface, which is placed at y = 0. Note that, despite using a model that neglects heat losses by convection and radiation, the quality of the fittings to Eq. 1 is very high, which indicates that the approximation is valid.

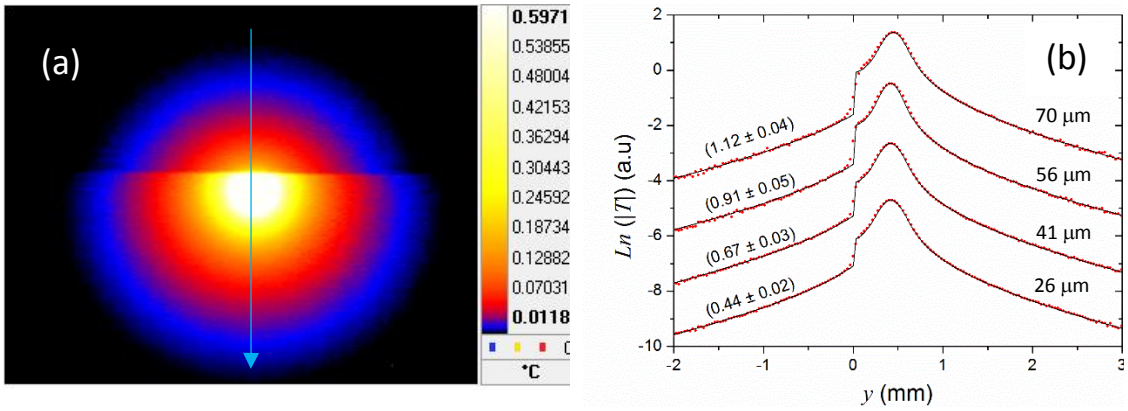

Fig. 6. (a) Amplitude thermogram for a water sample for a width L = 60 µm at a modulation frequency of f = 0.3 Hz. (b) Natural logarithm of the temperature amplitude profiles along the y-axis for four nominal widths and the same modulation frequency. The inserted values are the thermal resistances ($\times 10^{-4}$ m^2KW^{-1}) retrieved from the fit to Eqs. 1.

In Fig. 7 we show the results for ethylene-glycol. Measurements have been performed at f = 0.3 Hz. Figure 7a shows the amplitude thermogram recorded at L = 35 µm. Figure 7b shows the natural logarithm of the temperature amplitude profiles along the y-axis for four widths (L = 43, 35, 31 and 24 µm). Dots are the experimental data and the continuous lines are the fittings to Eqs. 1. The retrieved R_{th} values are inserted in the figure.

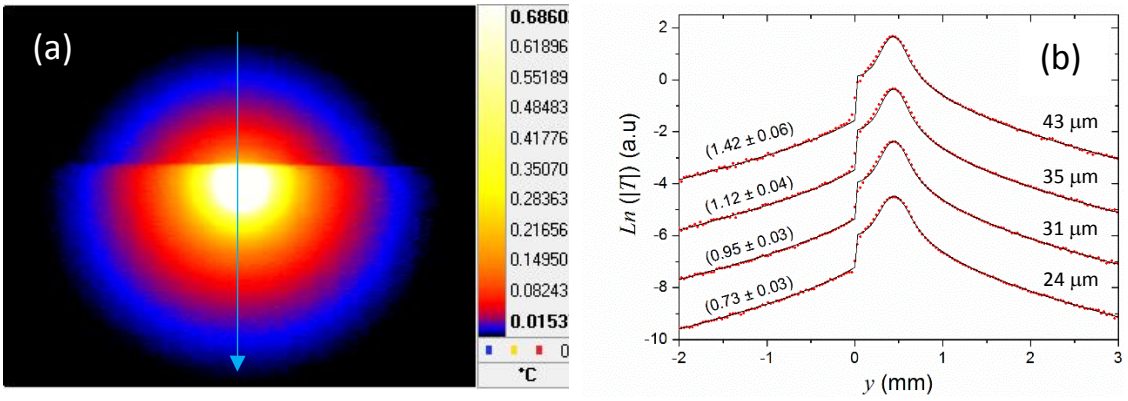

Fig. 7. (a) Amplitude thermogram for an ethylene-glycol sample for a width L = 35 µm, at a modulation frequency of f = 0.3 Hz. b) Natural logarithm of the temperature amplitude

profile along the *y*-axis for four nominal widths and the same modulation frequency. The inserted values are the thermal resistances ($\times 10^{-4}$ m^2KW^{-1}) retrieved from the fit to Eqs. 1.

Figure 8 shows the nominal L values as a function of the retrieved thermal resistance R_{th} for the experiments performed with water (a) and ethylene-glycol (b). The solid curves are the best linear fits of the data and the slope values give the thermal conductivity of the fluid: $k_{water} = 0.618 \pm 0.003$ $Wm^{-1}K^{-1}$ and $k_{ethylene\text{-}glycol} = 0.27 \pm 0.01$ $Wm^{-1}K^{-1}$. They are in good agreement with the literature values [7, 13]. As we can see, the measurement uncertainty in the fittings obtained with this improved configuration resulted in 1% and 4.6 % for the water and ethylene-glycol respectively, demonstrating the accuracy of the proposed method.

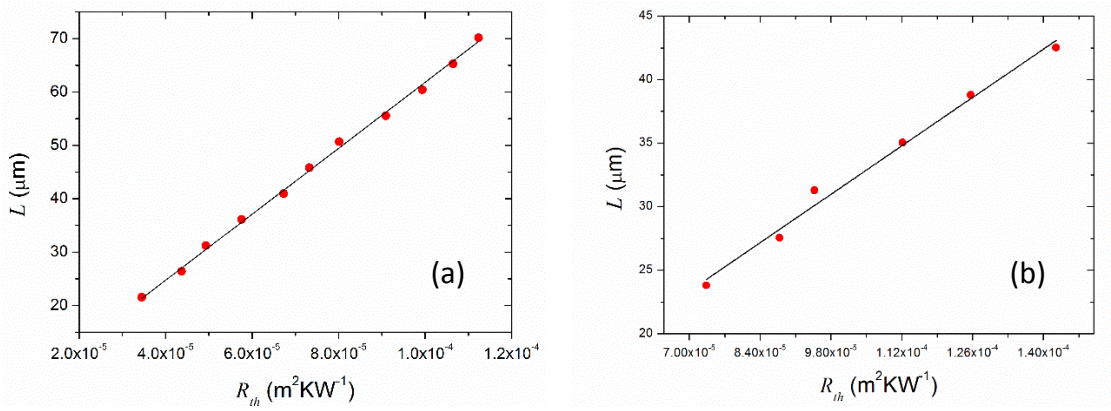

Fig. 8. Interface width as a function of the retrieved thermal resistance for water (a) and ethylene-glycol (b). The solid curves are the results of the best linear least squares fits.

5. Conclusions

A new method for thermal conductivity measurements in gases and liquids was proposed. It uses lock-in infrared thermography with laser spot heating for straightforward measurement of the thermal conductivity of gaseous and liquids samples that fill the gap layer between two solid materials. This is an accurate (measurement uncertainty below 5%), fast (measurement takes only some minutes) and non-contact method (both thermal excitation and detection involve electromagnetic waves) that requires very small quantity of sample (about 10^{-2} cm^3), so that it offers significant advantages if compared to the conventional techniques for thermal characterization of fluids such as the well-established hot wire method.

Acknowledgements

This work was partially supported by research grants from SIP-IPN (20181764, 20196720) and CONACyT (205640). The support of COFAA-IPN by the SIBE and BEIFI programs is also acknowledged. A.B. greatly thanks the support of CONACyT through the Beca Mixta Program for a research stay at the UPV/EHU and UPV/EHU support through "Ayuda para facilitar la estancia en la UPV/EHU de personas investigadoras en formación de países latinoamericanos matriculadas en las enseñanzas de doctorado de la UPV/EHU (2019)". Authors are also grateful for support by Ministerio de Economía y Competitividad (DPI2016-77719-R, AEI/FEDER, UE), by Gobierno Vasco (PIBA2018/15) and by Universidad del País Vasco UPV/EHU (GIU16/33).

References

[1] G. Paul, M. Chopkar, I. Manna, P.K. Das, Techniques for measuring the thermal conductivity of nanofluids: A review, Renewable and Sustainable Energy Reviews 14 (2010) 1913–1924

[2] M. J. Assael, K. D. Antoniadis, W. H. Wakeham, Historical Evolution of the Transient Hot-Wire Technique, Int. J. Thermophys. 31 (2010) 1051–72.

[3] M. Khayet, J. M. Ortiz de Zárate, Application of the Multi-current Transient Hot-Wire Technique for Absolute Measurements of the Thermal Conductivity of Glycols, Int. J. Thermophys. 26 (3) (2005) 637-646.

[4] W. A. Wakeham, M. J. Assael, Thermal conductivity measurement, In: Measurement, Instrumentation, and Sensors Handbook, J. G. Webster and H. Eren, CRS Press, (2018) 66.

[5] A. Cifuentes, A. Mendioroz, A. Salazar, Simultaneous measurements of the thermal diffusivity and conductivity of thermal insulators using lock-in infrared thermography, Int. J. Therm. Sci. 121 (2017) 305-312.

[6] J. González, A. Bedoya, A. Medioroz, A. Salazar, Measuring the thermal resistance of vertical interfaces separating two different media using infrared thermography, Int. J. Therm. Sci. 135 (2019) 410-416.

[7] D.P. Almond, P.M. Patel, Photothermal Science and Techniques Physics and Its Applications, Chapman and Hall, London, (1996) 17.

[8] Reported thermal conductivities of materials measured by different techniques can span a wide percentual range, as can be see for example in Y. S. Touloukian *et al*. Thermophysical properties of matter, v. 1. Thermal conductivity: metallic elements and alloys, (IFI/PLENUN: NY, 1970)

[9] M.L.V. Ramires, C. A. Nieto de Castro, Y. Nagasaka, A. Nagashima, M. J. Assael, W. A. Wakeham, Standard Reference Data for the Thermal Conductivity of Water, J. Phys. Chem. Ref. Data 24 (1995) 1377-1381.

[10] R.H. Bogaard, Thermal Conductivity of Selected Stainless Steels, In: Ashworth T., Smith D.R. (eds) Thermal Conductivity 18. Springer, Boston, MA (1985) 175-185.

[11] C.L. Choy, K.W. Kwok, W.P. Leung, F. P. Lau, Thermal conductivity of Poly (ether Ether Ketone) and its Short-Fiber Composites, J. Polym. Sci. Pol. Phys. 32 (1994) 1389-1397.

[12] R.H. Bogaard, P.D. Desai, H. H. Li, C. Y. Ho, Thermophysical properties of stainless steel, Themochim. Acta 218 (1993) 373-393.

[13] H. Xie, J. Wang, T. Xi, Y.Liu, F. Ai, Q. Wu, Thermal conductivity enhancement of suspensions containing nanosized alumina particles, J. Appl. Phys. 91 (7) (2002) 4568-4572.

[14] Breitenstein O, Langenkamp M. Lock-in thermography. Berlin: Springer; 2003.